# The abundance of unknots in various models of polymer loops



2006 J. Phys. A: Math. Gen. 39 9081

(http://iopscience.iop.org/0305-4470/39/29/005)

INSTITUTE OF PHYSICS PUBLISHING JOURNAL OF PHYSICS A: MATHEMATICAL AND GENERAL

J. Phys. A: Math. Gen. **39** (2006) 9081–9092 doi:10.1088/0305-4470/39/29/005

# The abundance of unknots in various models of polymer loops

**N T Moore**[1] **and A Y Grosberg**[2]

[1] Physics Department, Winona State University, Winona, MN 55987, USA
[2] Department of Physics, University of Minnesota, Minneapolis, MN 55455, USA

E-mail: nmoore@winona.edu and grosberg@physics.umn.edu

Received 8 April 2006
Published 5 July 2006
Online at stacks.iop.org/JPhysA/39/9081

**Abstract**

A veritable zoo of different knots is seen in the ensemble of looped polymer chains, whether created computationally or observed *in vitro*. At short loop lengths, the spectrum of knots is dominated by the trivial knot (unknot). The fractional abundance of this topological state in the ensemble of all conformations of the loop of $N$ segments follows a decaying exponential form, $\sim\exp(-N/N_0)$, where $N_0$ marks the crossover from a mostly unknotted (i.e., topologically simple) to a mostly knotted (i.e., topologically complex) ensemble. In the present work, we use computational simulation to look closer into the variation of $N_0$ for a variety of polymer models. Among models examined, $N_0$ is smallest (about 240) for the model with all segments of the same length, it is somewhat larger (305) for Gaussian-distributed segments, and can be very large (up to many thousands) when the segment length distribution has a fat power-law tail.

PACS numbers: 02.40.−k, 82.35.−x
Mathematics Subject Classification: 57M25, 82D60

(Some figures in this article are in colour only in the electronic version)

## 1. Introduction: formulation of the problem

Of interest to anglers seeking to fill their creels and children seeking to fasten their shoes, a wide audience has found knots compelling from time immemorial. In the scientific community, knots have been featured in initial formulations of the nature of atoms [1] (see a popular historical account in [2]), the formulation of certain path integrals [3] and also in quantitative biology, where knots have been observed in [4, 5] and tied into DNA [6, 7], where the space of knots is biologically created and manipulated [8]. Knots also have been observed occasionally in proteins [9–14].

  

Historically, the classification of knots and study of knot invariants were the first subjects of knot theory [2], and this remains the centre of attention among knot theorists of mathematical orientation [3]. Another fundamental aspect of knot theory is that of knot entropy. Physically, this group of problems comes to the fore in the context of polymers and biophysics. Mathematically, this issue belongs to both topology and probability theory and seems to remain underappreciated in the mathematics and mathematical physics community. Even the simplest question in this area is poorly understood: what is the probability that a randomly closed loop in 3D will be topologically equivalent to a plane circle? In other words, using professional parlance of the field, what is the probability that random loop is a trivial knot (unknot), $0_1$? There are, of course, many more questions along the same lines, e.g., what are probabilities of other more complex knots? what is the entropic response of a topologically constrained loop to various perturbations, etc.

Most of what we know about these 'probabilistic topology' questions is learned from computer simulations. In particular, it has been observed by many authors over the last three decades [15–19] that the trivial knot probability depends on the length of the loop, decaying exponentially with the number of segments in the loop, $N$:

$$w_{\text{triv}} = A \exp(-N/N_0). \tag{1}$$

For some lattice models this exponential law, in the $N \to \infty$ asymptotics, was also mathematically proven [20, 21]. It was also noted [17] that the same exponential law, with the same decay parameter $N_0$, also describes the large $N$ asymptotical tail of the abundance of any other particular knot—although for complex knots exponential decay starts only at sufficiently large $N$ (as soon as the given knot can be identified as an underknot [24]).

An alternative view of formula (1), useful in the context of thermodynamics, implies that the removal of all knots from the loop is associated with thermodynamically additive (linear in $N$) entropy loss of $1/N_0$ per segment; in other words, at the temperature $T$, untying all knots would require mechanical work of at least $k_B T/N_0$ per segment.

Another manifestation of the importance of the $N_0$ parameter was found in the recent series of works [22–25]. These works belong to the direction [26–30] addressing the spatial statistics of polymer loops restricted to remain in a certain topological knot state. It turns out that even for loops with no excluded volume and thus are not self-avoiding, $N_0$ marks the crossover scale between mostly Gaussian ($N < N_0$) and significantly non-Gaussian ($N > N_0$) statistics. Indeed, at $N < N_0$, locking the loop in the state of an unknot excludes only a small domain of the conformational space which produces only marginal (albeit non-trivial [25]) corrections to Gaussian statistics—for instance, mean-squared gyration radius of the loop is nearly linear in $N$. By contrast, at $N > N_0$, the topological constraints are of paramount importance, making the loop statistics very much non-Gaussian and consistent with effective self-avoidance [23, 24, 26, 30].

Thus, it seems likely that the parameter $N_0$ might hold the key to the entire problem of knot entropy. We therefore decided to look at this parameter more closely in this paper.

Present understanding of the values of $N_0$ is quite modest. First, the constant's value was invariably found to be quite large, around 300 for all examined models of 'thin' loops with no excluded volume, or no self-avoidance [15–17, 23, 24]. Second, it is known that knots are dramatically suppressed for 'thick' self-avoiding polymers, which means that $N_0$ rapidly increases with the radius of self-avoidance [17, 19]. The latter issue is also closely connected to the probabilities of knots in lattice models, where the non-zero effective self-avoidance parameter is automatically set by the lattice geometry. In the present paper, we will only consider the arguably more fundamental case of loops with self-avoidance excluding a negligible volume.

The starting point of our analysis is the observation that $N_0$ appears to be noticeably different for two standard polymer models for which common sense suggests that they should be equivalent. Both models can be called freely jointed in the sense that they consist of $N$ rigid segments with free rotation in the joints. However, in one model all segment vectors are of the same length, while in the other model segment vectors are taken from a Gaussian distribution. The motivation to consider the Gaussian-distributed step vectors comes from the idea of decimation or renormalization: we can start from the loop with $Ng$ segments of equal length and then group them into $N \gg 1$ blobs of $g \gg 1$ bare segments, each blob having nearly Gaussian-distributed end-to-end vector. With respect to the knot abundance, the fixed length model was examined in [16] and the Gaussian model in [17]. It was noted that $N_0$ for the Gaussian-distributed steps was larger than for identical steps, assuming no self-exclusion in both cases. No attention was paid to this observation, possibly because there was no confidence that the observed difference is real, in the context of the numerical error bars in the pertinent measurements.

Recently [23, 25], more detailed data became available which suggests that indeed $N_0$ is different for the two models, with fixed or Gaussian-distributed steplength. A similar result was independently obtained by Vologodskii [31]. Later in this paper, we present even better quality data supporting the same observation that $N_0$ is different for these two models. This is a rather disturbing observation. Indeed, the idea of universality in polymer physics [34] suggests that there should not be any difference between these two models as far as any macroscopic quantity is concerned. For instance, not only is the mean-squared gyration radius the same for both models, but even the distribution of the gyration radii is the same, except far into the tails. In general, the difference between polymer models of this type becomes significant only in the strong stretching regime [35] or at high density [32]. Even if one takes into account the idea that knots, when present in a low-density, swollen coil, are most likely localized along the chain [36–40], it is unclear how this fact can manifest itself for the loop which has no knots. (Here, it is worth noting in passing that knots are localized in swollen coils, but get delocalized along the chain when the polymer is a collapsed globule [41]; of course, this also does not seem to reflect on the swollen loops with no knots.)

Thinking generally about the loop models with fixed or Gaussian steplength, our reaction to this discrepancy is to realize that the major difference between the two freely jointed loop models is that the Gaussian model may have a few unusually long segments, suppressing the ability of other shorter segments to wind around, and thus decreasing the possibility for knots to occur, and accordingly, increasing $N_0$. Thus, the ability to take long strides might account for the comparative slowness of the ensemble of loops with Gaussian steplengths to diversify their knot spectrum with increasing $N$. The main goal of the present work is to investigate this conjecture.

The plan of the work is as follows. After a brief description of our computational algorithms used to generate closed loops and to identify their topologies (section 2), we present computational results (section 3) on knot abundance for a variety of models differing in the width of their steplength distribution. In addition to the already mentioned loops with fixed and Gaussian-distributed steplengths, in order to look at the even broader distributions which allow for very long segments, we also generated loops with the generalized Cauchy–Lorentz 'random-flight' distribution. Finally, we include loops of bimodally distributed fixed steplength.

In brief, our results are as follows. First, we confirm the exponential decay law of the unknot probability, formula (1), across all models examined. Second, we qualitatively find that indeed a wider distribution of the segment lengths leads to knot suppression, i.e. a larger $N_0$. Third, and most unexpectedly, we find that $N_0$ does not show any signs of any singular

behaviour associated with the divergence of mean-squared segment length or any other moment of the segment length distribution. Instead, $N_0$ blows up and appears to grow without a bound when the distribution of segment lengths approaches the border of normalizability.

## 2. Models and simulation methods

### *2.1. Models*

All polymer models referenced and employed in this work use a freely jointed model to represent a polymer loop. The polymer is represented by a set of $N$ vertices in 3D, with position vectors $\vec{x}_i$, where the step between successive vertices is described, $\vec{r} = \vec{x}_{i+1} - \vec{x}_i$. In all models, we assume that the distribution of segment vectors $\vec{r}$, which we call $P(\vec{r})$, is spherically symmetric and depends only on the steplength $r = |\vec{r}|$, such that

$$\langle \vec{r} \rangle = \int \vec{r}\, P(r)\, \mathrm{d}^3 r = 0. \tag{2}$$

We also assume that the mean-squared steplength is always the same (when defined!—see below), we denote it by $\ell$:

$$\langle r^2 \rangle = \int r^2 P(r)\, \mathrm{d}^3 r = 4\pi \int_0^\infty r^4 P(r)\, \mathrm{d}r = \ell^2. \tag{3}$$

With this in mind, the simplest measure of the distribution breadth involves higher order moments:

$$\sigma^2 = \frac{\langle r^4 \rangle - \langle r^2 \rangle^2}{\langle r^2 \rangle^2}, \tag{4}$$

where $\langle r^4 \rangle = 4\pi \int_0^\infty r^6 P(r)\, \mathrm{d}r$.

Specifically, we analysed the following models.

The *fixed steplength model* is described by the distribution

$$P(\vec{r}) = \frac{\delta(|\vec{r}| - \ell)}{4\pi \ell^2}. \tag{5}$$

For this model, of course $\sigma = 0$. With $N$ segments, the loop's contour length is obviously $L = N\ell$ and the mean-squared gyration radius of the loop is $\langle R_g^2 \rangle = (N+1)\ell^2/12$.

The *Gaussian steplength model* is generated by the distribution

$$P(\vec{r}) = \left(\frac{3}{2\pi \ell^2}\right)^{3/2} \exp\left[-\frac{3r^2}{2\ell^2}\right], \tag{6}$$

in this case, $\sigma = \sqrt{2/3}$. The contour length of the $N$-segment loop in this model is $L = N\langle |\vec{r}| \rangle = N\ell\sqrt{8/3\pi}$ and the mean-squared gyration radius is $\langle R_g^2 \rangle = (N - 1/N)\ell^2/12$.

The *random-flight steplength model* is obtained from the generalized Cauchy–Lorenz distribution (also known in the theory of Lévy flights [50]) of the form

$$P(\vec{r}) = \frac{\alpha \sin[3\pi/\alpha]/(4\ell^3\pi^2)}{1 + (r/\ell)^\alpha}, \tag{7}$$

where the factor in the numerator ensures normalization. Here, $\alpha$, a parameter of the distribution, must be greater than 3, otherwise the normalization integral diverges. Nevertheless, it would be fair to speak about a family of random-flight models, parameterized by $\alpha > 3$, instead of just one model. Varying $\alpha$ allows us to work with a 'tuneable' distribution. These distributions' 'fat' power-law tails lead to diverging moments (which is why they are used to describe super-diffusive behaviour seen in biological foraging [43–48],

and quite recently, in the diffusion of bank notes across the United States, [49]). Specifically, the ensemble-averaged contour length of the loop is well defined only at $\alpha > 4$ ($L = N\ell \sin(3\pi/\alpha)/\sin(4\pi\alpha)$), mean-squared gyration radius exists at $\alpha > 5$ and $\sigma$ only exists at $\alpha > 7$, in which case it is equal to

$$\sigma = \sqrt{\frac{\sin[5\pi/\alpha]^2}{\sin[3\pi/\alpha]\sin[7\pi/\alpha]} - 1} \qquad (\text{at } \alpha > 7). \tag{8}$$

Finally, we also include loops with *bimodally distributed steplength*. For these loops,

$$P(\vec{r}) = P_1 \frac{\delta(|\vec{r}| - \ell_1)}{4\pi\ell_1^2} + P_2 \frac{\delta(|\vec{r}| - \ell_2)}{4\pi\ell_2^2}, \tag{9}$$

which means that two possible steplengths, $\ell_1$ or $\ell_2$, occur with probabilities $P_1$ and $P_2$, subject to the normalization conditions, $P_1 + P_2 = 1$, and $\langle r^2 \rangle = P_1\ell_1^2 + P_2\ell_2^2 = \ell^2$. All bimodally distributed models can be conveniently parameterized by $P_1$ and $\lambda = \ell_2/\ell_1$. For these models,

$$\sigma = \sqrt{\frac{P_1 + (1 - P_1)\lambda^4}{(P_1 + (1 - P_1)\lambda^2)^2} - 1} \tag{10}$$

might be very large if $\lambda$ is very large and $P_1$ is rather close to unity ($\lambda^2 \gg 1/(1 - P_1) \gg 1$).

### *2.2. Loop generation*

Unbiased generation of closed loops is of decisive importance for our work. Recently, we gave a detailed review of the existing computational methods to generate statistically representative closed loops (see the last section of the work [25]). In principle, the best way to generate loops is based on the so-called conditional probability method. The idea is that a closed path is generated as a random walk, step by step, except after the completion of $k$ steps, the next step, $k + 1$, is generated from the analytically computed conditional probability distribution of the step vector $\vec{r}$, subject to the condition that after $N - k$ more steps, the walker returns to the starting point. This idea was first suggested and implemented for Gaussian-distributed steps [42]. Recently, we implemented this method for steps of equal length [25]. Unfortunately, this method is computationally costly and appears to be prohibitively difficult to implement for more sophisticated models, such as random flight.

We therefore use the simpler method, called the method of triangles. This method [23–25] generates loops of $N$ segments with $N$ divisible by 3. It involves creating a set of $N/3$ equilateral triangles, each randomly oriented in 3D space. Each triangle is considered a triplet of vectors with zero sum. A random permutation of the $N$ edge vectors which make up these $N/3$ triangles, and then connecting all $N$ vectors head-to-tail, creates a loop which will be closed, as the $N$ bond vectors together have 0 vector sum. Of course, this method imposes correlations between segments. We therefore take special care to compare the results of this method with the unbiased generation using the conditional probability method for both Gaussian distributed and equal length step models. We found that no appreciable deviations in knot abundance data arise from the imperfection of the triangle method. We therefore use the method of triangles to generate the random flight and bimodal-distributed loops, for which no alternative method is available. To avoid even the slightest problems with correlations, implicit in our triplet method, and to ensure that the decay of trivial knot probability is in the exponential regime, we exclude the data from small loops and fit the trivial knot probability on the interval $N \in [50, 300]$.

In the specific case of Lévy flights, or possibly in the case of bimodal steps when $P_1$ is near the bounds of definition, $1 - P_1 \ll 1$ or $P_1 \ll 1$, we admit the possibility that an

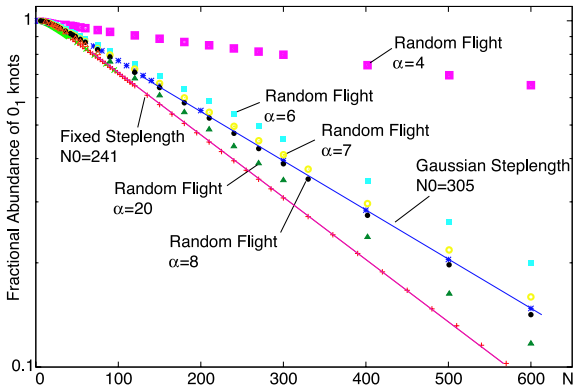


**Figure 1.** The fraction of loops of $N$ segments with trivial topology ($0_1$ or unknots) follows the decaying exponential form given in equation (1), as seen in this semi-logarithmic plot. The value of the decay constant $N_0$ varies considerably as the loop structure is changed. This figure displays the fraction trivially knotted for loops of fixed or Gaussian-distributed steplengths. The incongruity of $N_0$ between these two models, which for a variety of metrics are indistinguishable at large loop lengths, is apparent. The figure also shows data for a modified random-flight model, equation (7). In this model, the value of $N_0$ is tuneable by way of the parameter $\alpha$, which allows a substantial range of $N_0$ values, as indicated in the plot. The other model studied has bimodal distribution of steplengths, as described in section (3.3), and although not shown in the figure, allows similar variability in the decay length $N_0$.

exceptionally long segment will not occur singly in the loop but rather three times because of the nature of the triplet generation method. While this is an unfortunate artefact of triplet generation with unknown ramification, we know of no conditional probability formulation for the loop of Lévy-distributed steps. It would be interesting to address the Monte Carlo dynamics generation of loops with the Levy segment distribution. We stress however that the steplengths used for each triplet are selected from the proper Lévy distribution and, in terms of relative probabilities, no steplength in any loop is unduly weighted. As with intersegment correlation, we expect this problem to be damped out with increasing loop length.

### *2.3. Identification of topology and statistics*

For each of the models listed above, we generated loops of up to at least $N = 300$ segments.

Once the loop was generated, its knotted state was assessed computationally with the Alexander determinant, $|\Delta(-1)|$, as well as the Vassilev invariants of degrees 2 and 3, $v2$ and $v3$. For this purpose, we employed knot analysing routines described in detail elsewhere [33].

The fraction of generated loops with trivial topology was recorded for each loop type. In the interval $50 \leqslant N \leqslant 300$, every sample consisted of at least $10^6$ loops. As a result, the plot of trivial knot probability was created for each model, with statistical error bars smaller than the data points in figure 1. Based on the data, $N_0$ was measured for every model in our repertoire.

## 3. Results

Our main results are shown in figure 1. There, we present the semi-log plots of the data on the trivial knot probability as a function of the number of segments $N$ for a variety of models. To begin with, all our data agree quite well with the exponential character of the $w_{\mathrm{triv}}(N)$

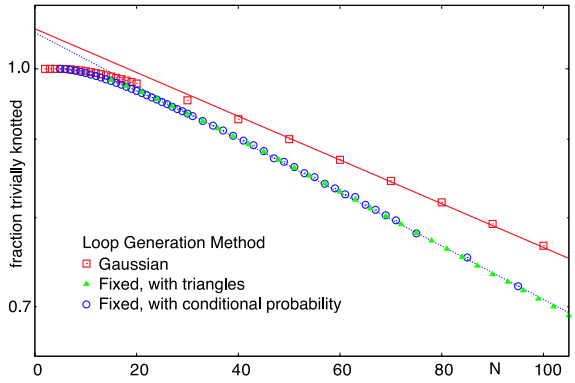


**Figure 2.** Semi-log plots of trivial knot probability against the number of segments for the Gaussian-distributed steplength model (□) and for the fixed steplength model, the latter generated either via conditional probability method (○) or triangles method (△). The results indicate no dependence on the generation method, thus lending credence to the simpler method of triangles. The results also indicate an almost perfect fit to the exponential law, equation (1), with $N_0 \approx 240$ for fixed steplength and $N_0 \approx 305$ for Gaussian-distributed steps.

dependence, formula (1). Our main emphasis is therefore the study of the characteristic value of $N_0$ for various models.

### *3.1. Loops of fixed steplength versus Gaussian-distributed steplength*

Let us start with the two most commonly used models. In the case of fixed length steps, we obtain $N_0 \approx 240$ (see also [23]). By contrast, for Gaussian-distributed length steps we get $N_0 \approx 305$ (see [25]).

All data for the Gaussian model were generated using the fundamentally unbiased conditional probability method. For the model with fixed length steps, we compare in figure 2 the data obtained by the conditional probability method [25] and data generated by the much more efficient method of triangles (see section 2.2). As the figure indicates, there is practically no visible difference in the results. Accordingly, we unreservedly rely on the triangles method in the rest of this work.

Although our main attention in this paper is on the trivial knots (unknots), we show in figure 3 some data for more complex knot probabilities. Our data at least do not contradict the assertion that the probability of every particular knot decays exponentially at sufficiently large $N$, with the same decay length as the trivial knot probability. At the same time, our data also confirm the systematic difference between models—decay length, although the same for all types of knots, does depend on the distribution of steplengths involved. Specifically, probabilities of knots $3_1$ and $4_1$ decay at a noticeably slower rate for the Gaussian model than for the model with fixed steps.

### *3.2. Random-flight loops*

The results of our study of loops with random-flight steplength, $\alpha \in [3.5, 30]$, are summarized in figures 1 and 4. The raw curves of probability given in figure 1 clearly show that the odds of finding an unknot in a set of loops get increasingly unfavourable as $\alpha$ decreases. That is not unexpected: at smaller $\alpha$, the probability distribution (7) acquires an increasingly fat tail, which implies the presence of a fraction of exceptionally long segments, and they of course suppress the chance of knots.

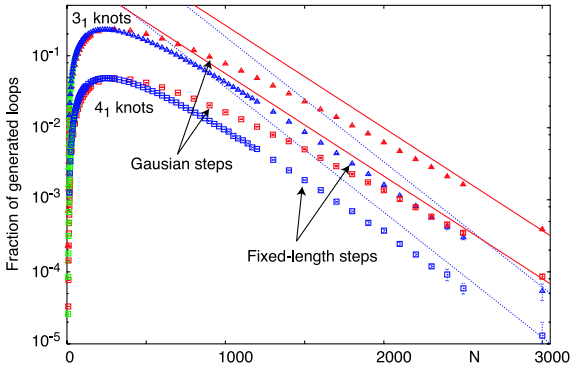


**Figure 3.** The probabilities of simple non-trivial knots $3_1$ and $4_1$ are plotted against the number of segments in the loop in semi-log scale. The data at large $N$ are consistent with the exponential form of these probabilities (plotted as solid lines in the figure), which are characterized by the same parameter $N_0$ found for trivial knots. As with the case of trivial knots, we see the difference between the fixed steplength model and Gaussian-distributed model, namely, that any particular knot probability decays slower for Gaussian-distributed segments than for fixed segments.

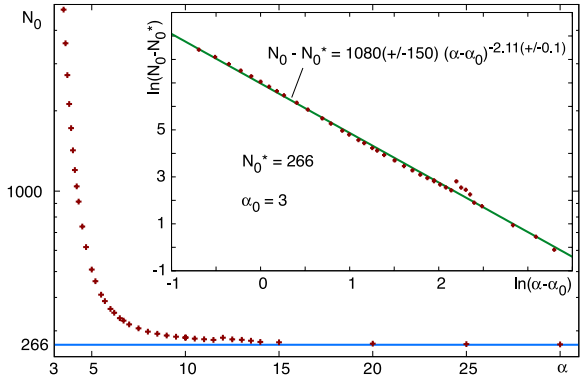


**Figure 4.** Values of the trivial knot decay length, $N_0$, measured from loops constructed of steps with generalized Cauchy–Lorenz distribution (reminiscent of Lévy flights). The decay constant is expressed as dependent on the variable $\alpha$ which defines how fat the tail of the distribution remains at large steplengths. The knot probability decay constant, $N_0$, approaches a constant value of about 266 at large $\alpha$. The inset shows the same data in double logarithmic scale. It is seen that $N_0$ blows up approximately as $(\alpha - 3)^{-2}$ when $\alpha$ decreases. It is interesting to note that the dependence of $N_0$ on $\alpha$ does not show any signs of irregularity as $\alpha$ crosses values at which various moments of segments length distribution start diverging (for instance, mean-squared gyration radius diverges at $\alpha \leqslant 5$ and mean contour length diverges at $\alpha \leqslant 4$).

At very large $\alpha$, the knot probability for the random-flight model appears similar to the data for fixed steplength loops. Indeed, as figure 4 indicates, $N_0$ for the random-flight model at very large $\alpha$ approaches $N_0 \approx 266$ which is not dramatically different from $N_0 \approx 240$ for the fixed length steps. In fact, the remaining difference might be associated with the fact that even at very large $\alpha$, the random-flight model, although it has essentially no very long steps, has some relatively short ones, which might account for the discrepancy in $N_0$. Figures 1 and 4 show further that at $\alpha \approx 7.5$, the random-flight loops behave essentially the same way as Gaussian steps in terms of $N_0$.

Most interestingly, figure 4 shows no sign of anything unusual happening to $N_0$ at the values of $\alpha$ at which various physically important moments of the segment length

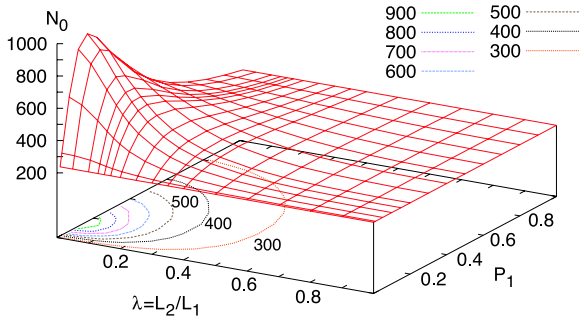


**Figure 5.** The surface plot of $N_0$ measured for loops of bimodally distributed steplength. The two steplengths used, $\ell_1$ and $\ell_2$, related by $\lambda = \ell_2/\ell_1$, occur with probabilities $P_1$ and $P_2$. The surface is described by two degrees of freedom, $\lambda$ and $P_1$. The model reduces to the fixed steplength model of section 3.1 under the conditions $P_1 = 0$ or $P_1 = 1$ or $\lambda = 1$, as is seen by the reduction of $N_0 \to 241$ in these limits. Interestingly, the bimodal distribution of steplengths never reduces $N_0$ below the limit of $N_0 = 241$ of the fixed steplength model. The maximum value of $N_0$ which we were able to observe, $N_0 = 974$, occurs at $P_1 = 0.15$, $\lambda = 0.01$.

distribution (7) start diverging. For instance, at $\alpha \leqslant 5$ the mean-squared gyration radius diverges, at $\alpha \leqslant 4$ even the contour length of the loop diverges—and yet none of these facts find any visible reflection on the dependence of $N_0$ on $\alpha$. $N_0$ keeps smoothly increasing with $\alpha$, with a maximum measured value of $N_0 \approx 4800$ at $\alpha = 3.5$. It appears that $N_0$ in fact blows up and goes to infinity as $\alpha$ approaches 3—the border below which the distribution (7) is not normalizable. Moreover, as the inset of figure 4 shows, this divergence is well approximated by the power-law dependence of the form

$$N_0 = N_0^* + B(\alpha - \alpha^*)^{-\beta}, \qquad \text{where} \quad N_0^* \approx 266, \quad B \approx 1080 \pm 150, \quad \alpha^* = 3 \quad \text{and} \quad \beta \approx 2.1 \pm 0.1. \tag{11}$$

In fitting the data with this power law, we ignored the small irregularities visible around $\alpha \approx 13$ (or $\ln[\alpha - \alpha_0] \approx 2.2$), which we attribute to the numerical problems with the cut-off implemented in our use of equation (A.1).

The meaning and physical origin of the apparent criticality observed at $\alpha$ approaching its minimal possible value of 3 currently evades our understanding.

### *3.3. Loops of bimodal-distributed steplength*

For this model, we examined the interval $N \in [50, 600]$, with at least $10^6$ loops in each simulation record for $N \leqslant 300$ and at least $10^5$ loops in those records used with length $N > 300$. We also consider parameters $P_1$ and $\lambda = \ell_1/\ell_2$ in the intervals $P_1 \in [0, 1]$ and $\lambda \in [0.01, 1.0]$, respectively. By symmetry, it is sufficient to look at $\lambda < 1$; this means, $P_1$ is the fraction of *shorter* segments.

The raw data from the loops with bimodal steplength are presented in figure 5. This surface plot charts the change in $N_0$ as a function of two parameters of the model, $P_1$ and $\lambda$. Below the surface is the corresponding contour plot of $N_0$ as a function of these two parameters. The changes in $N_0$ are smooth, and there do not seem to be any singularities in the behaviour of $N_0$. The maximum observed value of $N_0 = 974$ occurs at $P_1 = 0.15$, $\lambda = 0.01$. This maximum of $N_0$ appears to be rather sharp, small deviations in $P_1$ from 0.15 lead to smaller $N_0$ values. From the data, we believe that in this model $N_0$ is maximized when the fraction of shorter segments is $P_1 = 0.15 \pm 0.05$. As regards the second degree of freedom,

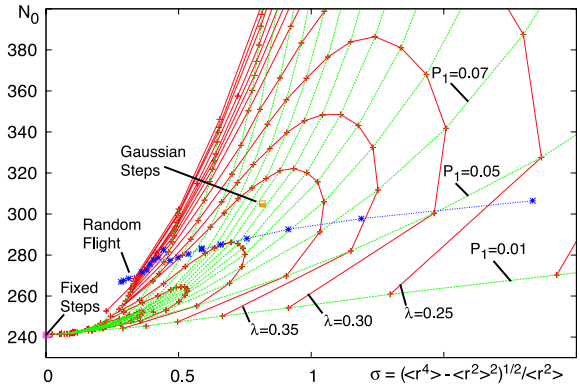


**Figure 6.** The value of $N_0$ for several different loop models is displayed against the steplength distribution width $\sigma$, which is defined in equation (4). The data in this figure fail the hypothesis that a larger $\sigma$ universally maps to a larger $N_0$. The measurement for fixed steplengths, shown in the lower left corner, is the point from which all bimodal loop data emanates. As labelled in the figure, the manifold for bimodal steplength is indexed by lines of constant $P_1$ and $\lambda$.

$\lambda$, while our data certainly shows that as $\lambda \to 1$ the bimodal system approaches the fixed steplength system of section 3.1 (i.e., $N_0 = 241$), in the opposite direction of $\lambda \to 0$, it is not clear if $N_0$ will continue to increase in an unbounded way or be in some way encumbered. In this regard, our present knot analysis machinery is limited by the relative disparity between segments of different lengths, and more work needs to be done to elucidate the scaling of $N_0$ in the limit $\lambda \to 0$.

Qualitatively, all of our data are consistent with the idea that what suppresses knots is the presence of a fraction of unusually long segments. One could then hypothesize that $N_0$ might depend on some unique property of the segment length distribution, for instance, $\sigma$, as defined in equation (4). This hypothesis is tested in figure 6; the figure indicates that the hypothesis fails. Nevertheless, the results presented in this figure are interesting, as they show that large $N_0$ can be achieved by the combination of segment length difference ($\lambda$) and segment-type fractions.

Although a functional relationship between $N_0$ and $\alpha$ seems evident in our data for random-flight loops, the data we have for loops with bimodal distribution of steplength do not suggest a simple single parameter which determines $N_0$.

## 4. Conclusions

In a qualitative sense, it does seem that there exists a relationship between $N_0$ and the reach of successive segments within the chain (as seen in figure 6). It seems qualitatively clear indeed that knottedness is greatly suppressed by the presence of some very long segments. Thus, the slowly decaying tail of the segment length probability distribution, or the presence of a small fraction of very long segments, implies a large $N_0$, which sounds natural. However, our understanding of these observations beyond the qualitative level is limited. We found that $N_0$ appears to exhibit no singularity associated with divergence of any natural characteristics of the loop, such as its gyration radius or even contour length; instead, $N_0$ exhibits power-law critical behaviour when the segment length distribution approaches the boundary of normalizability. In addition, we do not know which property of the segment length distribution determines $N_0$. We have established that this is not simply the distribution width, and from the results with

random-flight distribution it seems also clear that it is not based on any finite moments of the distribution. We consider the development of a fuller understanding of the variance of $N_0$ a compelling challenge.

The data clearly show that wide variation in the behaviour of $N_0$ is possible, including very large values of $N_0$ in certain models. Given that $N_0$ plays the role of the crossover length for the critical behaviour of topologically constrained loops [25], we can speculate that the models with very large $N_0$ are in some way similar to the models of self-avoidance in the vicinity of the $\theta$-point. We think that this analogy deserves very close attention.

## Acknowledgments

We acknowledge useful discussion with A L Efros and A V Vologodskii. We express thanks to R Lua for the use of his knot analysis routines. We are grateful for access to the Minnesota Supercomputing Institute's IBM Core Resources and the University of Minnesota Physics Department linux cluster, resources which made much of the simulation possible. This work was supported in part by the MRSEC Program of the National Science Foundation under Award Number DMR-0212302.

## Appendix. On the numerical implementation of generalized Cauchy–Lorenz distribution

To generate steplengths from the random-flight distribution (7), we first take a random number $q$ from the uniform distribution on the interval [0, 1] and then find steplength $r$ as $r = f(q)$, where the mapping $f(q)$ is determined by the equation

$$q = \int_0^{f(q)} P(\vec{r})\, 4\pi r^2\, \mathrm{d}r, \tag{A.1}$$

where $P(\vec{r})$ is given by equation (7). Although a closed-form representation of the right-hand side of equation (A.1) exists in the form of an incomplete beta function [51], we chose to implement the mapping via a numerical interpolation of tabulated values of the integral. As the power-law tail of this distribution is quite fat, particularly at small $\alpha$, accurate representation of the integral becomes challenging at large steplengths. This work is ultimately numerical, and we are forced to truncate the representation of the integral to 1.0 at some maximum steplength, i.e. specifying an upper bound on $f(q)$. The slow convergence of the tail is behind the appearance of the few outliers in the data for the random-flight method, see figure 4.

## References

[1] Lord Kelvin 1868 *Trans. R. Soc. Edinb.* **25** 217
[2] Silver D S 2006 *Am. Sci.* **94** 158–65
[3] Witten E 1989 *Commun. Math. Phys.* **121** 351–99
[4] Dean F, Stasiak A, Koller T and Cozzarelli N 1985 *J. Biol. Chem.* **260** 4975
[5] Rybenkov V, Cozzarelli N and Vologodskii A 1993 *Proc. Natl Acad. Sci. USA* **90** 5307
[6] Arai Y, Yasuda R, Akashi K, Harada Y, Miyata H, Kinosita K and Itoh H 1999 *Nature* **399** 446
[7] Bao X R, Lee H J and Quake S R 2003 *Phys. Rev. Lett.* **91** 265506
[8] Flammini A, Maritan A and Stasiak A 2004 *Biophys. J.* **84** 2968–75
[9] Mansfield M L 1994 *Nat. Struct. Biol.* **1** 213–4
[10] Taylor W R 2000 *Nature* **406** 916–9
[11] Zarembinski T I, Kim Y, Peterson K, Christendat D, Dharamsi A, Arrowsmith C H, Edwards A M and Joachimiak A 2003 *Proteins Struct. Funct. Genet.* **50** 177–83
[12] Takusagawa F and Kamitori S 1996 *J. Am. Chem. Soc.* **118** 8945–6

[13] Lua R C and Grosberg A Y 2006 *PLoS Comput. Biol.* **2** e45
[14] Virnau P, Mirny L and Kardar M 2006 Gordian Knot in human ubiquitin hydrolase *PLOS Computational Biology* at press
[15] Vologodskii A V, Lukashin A V and Frank-Kamenetskii M D 1974 The knot problem in statistical mechanics of polymer chains *Sov. Phys.—JETP* **67** 1875
[16] Koniaris K and Muthukumar M 1991 *Phys. Rev. Lett.* **66** 2211
[17] Deguchi T and Tsurusaki K 1997 *Phys. Rev.* E **55** 6245
[18] Janse van Rensburg E J and Whittington S G 1990 *J. Phys. A: Math. Gen.* **23** 3573–90
[19] Klenin K, Vologodskii A, Anshelevich V, Dykhne A and Frank-Kamenetskii M 1988 *J. Biomol. Struct. Dyn.* **5** 1173
[20] Sumners D W and Whittington S G 1988 *J. Phys. A: Math. Gen.* **21** 1689–94
[21] Pippenger N 1989 *Discrete Appl. Math.* **25** 273
[22] Grosberg A Y 2000 *Phys. Rev. Lett.* **85** 3858
[23] Moore N T, Lua R and Grosberg A Y 2004 *Proc. Natl Acad. Sci. USA* **101** 13431
[24] Moore N T, Lua R C and Grosberg A Y 2005 Under-knotted and over-knotted polymers: 1. Unrestricted loops *Physical and Numerical Models in Knot Theory, Including Applications to the Life Sciences (Series on Knots and Everything* vol 36*)* ed J A Calvo, K C Millet, E J Rawdon and A Stasiak (Singapore: World Scientific) pp 363–84
[25] Moore N T and Grosberg A Y 2005 *Phys. Rev.* E **72** 061803
[26] des Cloizeaux J 1981 *J. Phys. Lett.* **42** L433
[27] Quake S R 1994 *Phys. Rev. Lett.* **73** 3317
[28] Deutsch J M 1999 *Phys. Rev.* E **59** R2539
[29] Matsuda H, Yao A, Tsukahara H, Deguchi T, Furuta K and Inami T 2003 *Phys. Rev.* E **68** 011102
[30] Dobay A, Dubochet J, Millett K, Sottas P and Stasiak A 2003 *Proc. Natl Acad. Sci. USA* **100** 5611
[31] Vologodskii A V 2004 Talk given at *The Pittsburgh Meeting of American Mathematical Society, Session on Knots and Macromolecules (5–7 November 2004)*
[32] Grosberg A Y and Khokhlov A R 1994 *Statistical Physics of Macromolecules* (New York: AIP) p 91
[33] Lua R, Borovinskiy A and Grosberg A 2004 *Polymer* **45** 717
[34] De Gennes P G 1979 *Scaling Concepts in Polymer Physics* (Ithaca, NY: Cornell University Press)
[35] Bustamante C, Marko J F, Siggia E D and Smith S 1994 *Science* **265** 1599
[36] Lua R C, Moore N T and Grosberg A Y 2005 Under-knotted and over-knotted polymers: 2. Compact self-avoiding loops *Physical and Numerical Models in Knot Theory, Including Applications to the Life Sciences (Series on Knots and Everything* vol 36*)* ed J A Calvo, K C Millet, E J Rawdon and A Stasiak (Singapore: World Scientific) pp 385–98
[37] Metzler R, Hanke A, Dommesrnes P G, Kantor Y and Kardar M 2002 *Phys. Rev. Lett.* **88** 188101
[38] Hanke A, Metzler R, Dommesrnes P G, Kantor Y and Kardar M 2003 *Eur. Phys. J.* E **12** 347
[39] Orlandini E, Stella A L and Vanderzande C 2003 *Phys. Rev.* E **68** 031804
[40] Virnau V, Kantor Y and Kardar M 2005 *J. Am. Chem. Soc.* **127** 15102–6
[41] Marcone B, Orlandini E, Stella A L and Zonta F 2005 *J. Phys. A: Math. Gen.* **38** L15–21
[42] Vologodskii A V and Frank-Kamenetskii M D 1981 Topological aspects of polymer physics: theory and its biophysical applications *Sov. Phys. Usp.* **134** 641
[43] Viswanathan G M, Afanasyev V, Buldyrev S V, Havlin S, da Luz M G E, Raposo E P and Stanley H E 2001 *Braz. J. Phys.* **31** 102
[44] Levandowsky M, Klafter J and White B S 1988 *Bull. Marine Sci.* **43** 758
[45] Cole B J 1995 *Anim. Behav.* **50** 1317
[46] Boyer D, Miramontes O, Ramos-Fernandez G, Mateos J L and Cocho G 2003 *Priprint* cond-mat/0311252
[47] Focardi S, Marcellini P and Montanaro P 1996 *J. Anim. Ecol.* **65** 606
[48] Viswanathan G M, Afanasyev V, Buldyrev S V, Murphy E J, Prince P A and Stanley H E 1996 *Nature* **381** 413
[49] Brockmann D, Hufnagel L and Geisel T 2006 *Nature* **439** 04292
[50] Weisstein Eric W *Lévy Distribution* From MathWorld—A Wolfram Web Resource http://mathworld.wolfram.com/LevyDistribution.html
[51] Weisstein Eric W *Incomplete Beta Function* From MathWorld—A Wolfram Web Resource http://mathworld.wolfram.com/IncompleteBetaFunction.html